Additive-assisted synthesis and optoelectronic properties of $(CH_3NH_3)_4Bi_6I_{22}$

*Manila Sharma,[1] Aymen Yangui,[1] Alain Lusson,[2] Kamel Boukheddaden,[2] Xiaxin Ding,[4] Mao-Hua Du,[3] Krzysztof Gofryk,[4] Bayrammurad Saparov[1]**

[1]Department of Chemistry and Biochemistry, University of Oklahoma, 101 Stephenson Parkway, Norman, Oklahoma 73019, United States

[2]Groupe d'Étude de la Matière Condensée, CNRS-UMR8635, Université de Versailles Saint Quentin, Université Paris-Saclay, 45 Avenue des États-Unis, 78035 Versailles cedex, France.

[3]Materials Science and Technology Division, Oak Ridge National Laboratory, Oak Ridge, TN 37831, USA

[4]Idaho National Laboratory, Idaho Falls, ID 83415, USA

Corresponding Author

*E-mail: saparov@ou.edu

Abstract: Hybrid organic-inorganic halides containing Bi and Sb generally exhibit higher stability and lower toxicity compared to Pb analogues. In this work, synthesis, crystal and electronic structures and optical properties of a brand-new methylammonium bismuth iodide, $(MA)_4Bi_6I_{22}$ ($MA^+ = CH_3NH_3^+$), are reported. Interestingly, we find that the presence of the HgI_2 is necessary for the targeted preparation of $(MA)_4Bi_6I_{22}$. $(MA)_4Bi_6I_{22}$ contains isolated $[Bi_6I_{22}]^{4-}$ clusters made of six edge-sharing octahedral BiI_6 units, which are separated by MA^+ cations in its 0D crystal structure. A relatively low optical band gap of 1.9 eV was estimated for $(MA)_4Bi_6I_{22}$ based on diffuse reflectance measurements. An intense photoluminescence peak emerges at 636 nm at low temperatures that supports the assigned band gap value. Electronic structure calculations show the presence of flat bands in the valence and conduction bands, consistent with the low-dimensional structure of $(MA)_4Bi_6I_{22}$, and slightly indirect nature of the bandgap. Our findings suggest that the use of facilitator moieties such as HgI_2 may provide a pathway to obtaining alternative methylammonium bismuth iodides to $(MA)_3Bi_2I_9$.

Introduction

Iodometallates of heavy p-block elements with general formula $A_xM_yI_z$ (A = larger organic or inorganic cation such as Cs^+, methylammonium (MA^+)] or formamidinium (FA^+); M = divalent or trivalent cations Sn^{2+}, Pb^{2+}, Sb^{3+}, or Bi^{3+} have been widely investigated in recent years because of their remarkable optical and electronic properties.[1-3] These materials have been shown to exhibit bright luminescence,[4] ferroelectricity,[5] semiconducting[6] and nonlinear optical properties.[1, 7, 8] Among the iodometallates, $APbI_3$ have attracted most interest due to their outstanding performance in solar cell devices. Despite their remarkable solar cell performance with record efficiencies above 25%[9], the presence of toxic lead and instability of lead-based halides present major challenges for their commercialization.[10-12]

The search for environmentally-benign and higher stability alternatives to lead halides initially focused on Sn and Ge-based halides, however, the lighter tetrels Sn and Ge prefer tetravalent oxidation state rendering divalent tin and germanium halides chemically unstable.[13, 14] On the other hand, Sb and Bi halides based on Sb^{3+} and Bi^{3+} metal cations, which are isoelectronic to Sn^{2+} and Pb^{2+}, have also been proposed as potential alternatives to toxic lead halides.[15-17] However, the substitution of divalent Pb^{2+} with M(III) necessitates changes into the perovskite materials AMI_3 stoichiometry to maintain the charge balance. Thus, a recent survey of homometallic iodobismuthates and iodoantimonates show that the known compounds in these systems have I/M(III) ratios between 3.33 and 6, the latter corresponding to a 0D crystal structure containing isolated MI_6 octahedra.[1, 18, 19] Due to the increased I/M(III) ratios, these materials adopt low-dimensional (0-2D) crystal structures featuring isolated metal halide octahedra or 0D clusters of octahedra via corner-, edge- and face-sharing, 1D chains and rarely 2D layers.[18-22] Therefore, specific iodobismuthate structures can be conveniently targeted by controlling the loading ratio of reactants, however, the success of this approach greatly depends on the synthetic conditions (e.g., temperature, solvent effects etc.) and the type of A cation (e.g., size and shape of the organic A cation).

Among the iodobismuthates, $(MA)_3Bi_2I_9$ is a well-known 0D compound, which has been widely studied as a lower toxicity and higher stability alternative to $MAPbI_3$.[23-25] Despite promising early results on $(MA)_3Bi_2I_9$, further attempts to improve materials properties through discovery of new MA-Bi-I phases has been largely stagnant because $(MA)_3Bi_2I_9$ is a known high-stability phase in this phase diagram.[26] A recent work on the preparation of a heterometallic double perovskite $(MA)_2AgBiBr_6$ employed $PbBr_2$ additive in the reaction mixture to circumvent the formation of the high stability phase $(MA)_3Bi_2Br_9$, which forms in the absence of $PbBr_2$.[20] Initially, $PbBr_2$ was believed to form $MAPbBr_3$, which in turn acted as an *in situ* seed for perovskite-type crystal growth. However, follow-up studies suggest that the impurity additive plays a crucial role in the formation of intermediate species along the reaction pathway, which ultimately force the formation of the double perovskite product.[27] Importantly, the use of facilitator additives thus offers a brand-new approach for the preparation of otherwise inaccessible compounds in the MA-Bi-X phase diagrams. In this work, we report a new organic-inorganic iodobismuthate $(MA)_4Bi_6I_{22}$ featuring a 0D crystal structure based on isolated $[Bi_6I_{22}]^{4-}$ clusters. To the best of our knowledge, $(MA)_4Bi_6I_{22}$ is only the second compound in the MA-Bi-I phase diagram other than the well-studied high stability compound $(MA)_3Bi_2I_9$. In order to prepare $(MA)_4Bi_6I_{22}$, HgI_2 was used as a facilitator during our synthesis experiments. Our experimental work on $(MA)_4Bi_6I_{22}$ including X-ray diffraction, microscopy, thermal analysis and optical spectroscopy results are discussed in conjunction with density function theory (DFT) calculations.

Experimental

Chemicals. The chemicals used in this study (i) bismuth(III) iodide (anhydrous 99.998% powder, Sigma Aldrich), (ii) mercury iodide(99+%, Sigma Aldrich) (iii) hydroiodic acid (57 wt. % in H_2O, Sigma Aldrich), (iv) methylamine solution (40 wt. % in H_2O, Sigma-Aldrich), (v) absolute ethanol (200 proof, Sigma Aldrich) and (vi) acetone (Sigma-Aldrich) were used as received.

Synthesis of MAI. MAI was synthesized following a reported methods in literature.[19, 28] For this purpose, a methylamine solution was cooled to 0 ºC and stoichiometric amounts of HI (aq) was added dropwise under continuous stirring. The resultant solution was blended for up to 1.5 hr. Then, solvent was removed at 60 ºC, and the powder product was re-dissolved in ethanol to make a slurry. In the next step, addition of large excess of diethyl ether facilitated precipitation of MAI as a white powder product. The product was washed with benzene and ethanol, then vacuum dried overnight.

Synthesis of $(MA)_4Bi_6I_{22}$. A mixture of BiI_3 (0.1 mmol), MAI (0.1 mmol) and HgI_2 (0.1 mmol) was added to a Me_2CO/EtOH solvent system (15mL, 1:2 in volume). The resulting cloudy solution was filtered a using a 0.45-micron filter and supernatant was left in air after for crystal growth at room temperature. After keeping in air for about 1-day, red block crystals of $(MA)_4Bi_6I_{22}$ were formed (up to 0.5 cm in length) (see Fig. S1(a) in the Supporting Information file (SI)).

Microscopy. Optical microscopy images of $(MA)_4Bi_6I_{22}$ crystals (Fi. S1(a)) were taken using a Leica S6D microscope equipped with an EC4 camera. Energy Dispersive X-ray (EDX) spectroscopy measurements were performed on a Zeiss Neon EsB equipped with an Oxford Instruments EDX system. Elemental analysis of $(MA)_4Bi_6I_{22}$ crystals confirms the absence of Hg in the crystals and yields a I/Bi ratio of 3.33 (see Fig. S1(b)), which is close to the expected I/Bi ratio of 3.67.

Single Crystal X-ray diffraction. The single crystal X-ray diffraction experiments on $(MA)_4Bi_6I_{22}$ crystals were performed on a Bruker D8 Quest with a Kappa-geometry goniometer, an Incoatec Imus X-ray source (graphite-monochromated Mo-Kα (λ = 0.71073 Å) radiation), and a Photon II detector. For low temperature measurements, crystals were cut to suitable sizes in a Dow Chemical vacuum grease and cooled under a stream of nitrogen to 100(2) K. The crystals structure was determined from a non-linear least-squares fit. The data was corrected for absorption by the semi-empirical method based on equivalents and the structure was solved by direct methods by use of the SHELXTL program and refined by full matrix least-squares on F^2 by use of all reflections. All non-hydrogen atoms were refined with anisotropic displacement parameters, whereas all hydrogen atom positions were determined by geometry. Details of the crystallographic results are given in Table 1. Additional information on the crystal structure investigations at room temperature can be obtained in the form of a CIF (Crystallographic Information File), which was deposited in the was deposited in the Cambridge Crystallographic Data Centre (CCDC) database (deposition number 1963616).

Powder X-ray diffraction. Powder X-ray diffraction (PXRD) measurements were performed on a Rigaku MiniFlex600 system equipped with a D/tex detector using Ni-filtered Cu-Kα radiation source. Typical PXRD scans were collected in the 3-90° (2θ) range, with a step size of 0.2°.

Table 1. Selected single crystal data and structure refinement parameters for $(MA)_4Bi_6I_{22}$

Formula	$(CH_3NH_3)_4Bi_6I_{22}$
Formula weight (g/mol)	4173.95
Temperature (K)	100(2)
Radiation, wavelength (Å)	Mo Kα, 0.71073
Crystal system	Monoclinic
Space group, Z	$P2_1/c$, 2
Unit cell parameters	a = 17.733(3) Å
	b = 10.7585(12) Å
	c = 21.764(3) Å
	β = 112.733(5)°
Volume (Å^3)	3829.6(9)
Density (ρ_{calc}) (g/cm^3)	3.620
Absorption coefficient (μ) (mm^{-1})	22.613
$\theta_{min} - \theta_{max}$ (°)	2.26 – 27.48
Reflections collected	103503
Independent reflections	7259
R^a indices ($I > 2\sigma(I)$)	R_1 = 0.0263
	wR_2 = 0.0856
Goodness-of-fit on F^2	1.005
Largest diff. peak and hole (e$^-$/Å^3)	3.387 and -2.050

$^a R_1 = \sum\big||F_o| - |F_c|\big|/\sum|F_o|$; $wR_2 = |\sum|w(F_o^2 - F_c^2)^2|/\sum|w(F_o^2)^2||^{1/2}$, where $w = 1/|\sigma^2 F_o^2 + (AP)^2 + BP|$, with $P = (F_o^2 + 2F_c^2)/3$ and weight coefficients A and B.

Thermal properties. Simultaneous thermogravimetric analysis (TGA) and differential scanning calorimetry (DSC) measurements on polycrystalline samples of $(MA)_4Bi_6I_{22}$ were performed using a TA Instruments SDT 650 thermal analyzer system. The sample was heated at a rate of 5 °C/min from 25 °C to 600 °C under an inert flow of dry nitrogen gas. The heat capacity measurements were carried out in a Quantum Design Physical Property Measurement System (DynaCool-9) using the two-tau method.

Optical measurements. Room temperature diffuse reflectance spectrum was measured on a polycrystalline powder sample of $(MA)_4Bi_6I_{22}$ using a high-resolution PerkinElmer LAMBDA 750 UV–Vis–NIR spectrometer equipped with a 100 mm integrating sphere attachment combined with InGaAs photodetector. Photoluminescence spectra were measured on a single crystal using a double monochromator U1000 equipped with a photomultiplier. The excitation wavelength was the 325 nm line of a Spectra-Physics beamlock 2085 argon laser. The sample was placed in a helium bath cryostat and the measurements were performed between 2 and 150 K.

Electronic structure calculations. For electronic structure calculations, a model structure without a structural disorder was created by assigning full occupancies to higher site occupancy factor (SOF) crystallographic positions in split sites. All calculations were based on density functional theory (DFT) as implemented in the VASP code.[29] The kinetic energy cutoff of the plane-wave basis is 400 eV. The projector augmented wave method was used to describe the interaction between ions and electrons.[30] The band structure and the density of state of $MA_4Bi_6I_{122}$ were calculated using Perdew-Burke-Ernzerhof (PBE) exchange-correlation functional.[31] The lattice parameters were fixed at the experimentally measured values while the atomic positions were optimized[10] until the force on each atom is less than 0.02 eV/Å. The spin-orbit coupling (SOC) was included in all calculations.

Results & discussion

Synthesis and crystal structure.

$(MA)_4Bi_6I_{22}$ was first discovered while exploring the MA-Hg-Bi-I phase diagram to obtain heterometallic hybrid organic-inorganic halides.[3, 32] Subsequent stoichiometric reactions targeting

$(MA)_4Bi_6I_{22}$ in the absence of HgI_2 resulted in the high stability compound $(MA)_3Bi_2I_9$. Presence of impurity metal halides in solution mixtures is suspected to impact complex intermediates that can play decisive role in the preferred reaction pathways.[27] Existence of various bismuth halide clusters such as the hexanuclear $[Bi_4Hg_2I_{20}]^{4-}$ and trinuclear $[Bi_2HgI_{10}]^{2-}$ anions has already been demonstrated in literature.[3] However, in this case, the charge balance of the resultant compound according to $(MA^+)_4(Bi^{3+})_6(I^-)_{22}$ suggests absence of Hg^{2+} in the final product, which is also confirmed through EDX measurements (Fig. S1).

$(MA)_4Bi_6I_{22}$ crystallizes in the monoclinic space group $P2_1/c$ with a 0D crystal structure comprising isolated $[Bi_6I_{22}]^{4-}$ clusters separated by MA^+ cations (Fig. 1a). Each $[Bi_6I_{22}]^{4-}$ polyanionic cluster consists of six edge-sharing octahedral BiI_6 units (Fig. 1b). The polyanionic clusters are separated by methylammonium cations, which show rotational disorder (Fig. S2). Such rotational disorder is ubiquitous in hybrid metal halides containing small organic cations such as MA^+ cations and can lead to multiple order-disorder transitions. For example, the structure of the related compound $(MA_3)Bi_2I_9$ has also been is modelled as C and N superimposed on each other with a 50/50 occupancy on each site.[33] Computational studies have shown that orientational disorder of the MA^+ dipoles in the crystal structure can impact the conduction and valence band edges in $MA_3Bi_2I_9$.[34] More in-depth structural studies have been carried out for $MAPbI_3$, which show that MA^+ cations are fully ordered in the orthorhombic phase at low temperatures around 10 K.[35] Upon heating, there is a significant enhancement in the thermal motion of MA^+ cations as evidenced by enlarged atomic displacement parameters (ADPs) at 130 K in the orthorhombic phase. Further heating results in structural transition to a tetragonal phase, which exhibits partially ordered MA^+ cations. Based on quasielastic neutron scattering measurements, the MA+ cations have been shown to be in dynamic disorder in this structure. Finally, the high temperature cubic phase of $MAPbI_3$ exhibits fully disordered MA^+ cations.[35]

Analogous 0D structures with the $[Bi_6I_{22}]^{4-}$ polyanionic cluster were also previously reported for compounds containing much larger organic cations such as the dication based on the alkylamine 1,3-bis-(4-piperidyl)propane (H_2TMDP^{2+})[36] and PEt_4^+.[37, 38] Interestingly, alternative polyanionic structures exist with the same I/M(III) ratio of 3.67 (i.e., with the $[Bi_3I_{11}]^{2-}$ or $[Bi_6I_{22}]^{4-}$ formulas),[18, 37, 39] which can be explained through the templating role of the cations used in each specific case. Notwithstanding this fact, even for the same cation H_2TMDP^{2+}, two different polyanionic structures can be obtained if different loading ratios of reactants BiI_3 and the organic salt are used; higher bismuth iodide loading typically yields more condensed anionic networks.[18, 36] In addition, solvent incorporation into the crystal structures have been observed for several iodobismuthates under solvothermal synthesis conditions.[36] Thus, in combination with our synthesis experiments, analysis of the crystal structure of $(MA)_4Bi_6I_{22}$ and related iodobismuthates suggest that the details of solution preparation of iodometallates not only impacts the accessibility of various compositions but also the resultant crystal structures.

The BiI_6 octahedra are highly distorted with Bi – I bond lengths varying from 2.8522 (6) to 3.3957(7) Å and I – Bi – I bond angles from 82.790(16) to 94.39(2)° (Table S1). Within individual octahedra, the terminal $Bi\text{-}I_{terminal}$ contacts are shorter (~2.9 Å) than the sum of the Shannon ionic radii bismuth(III) and iodide (3.23 Å),[40] whereas the bridging $Bi\text{-}I_{bridging}$ can be as long as 3.3957(7) Å. The observed bond distances and angles in $(MA)_4Bi_6I_{22}$ are comparable to that reported for the related iodobismuthates.[36, 39] Octahedral distortions in hybrid organic-inorganic iodobismuthates are typically attributed to either stereochemically active lone pair $6s^2$ electrons on Bi^{3+} or the impact of hydrogen bonding between the organic and inorganic structural units.[1, 18] In related iodobismuthates, such observed distortions were judged as too insignificant to arise from the localization of lone pair.[36] We note here that in metal halide perovskites literature, comparable distortions have been attributed to the stereoactivity of lone ns^2 pairs on metals.[1, 18] In fact, the most likely scenario includes simultaneous contributions of the stereoactive lone ns^2 pairs, hydrogen bonding interactions between the organic cation and inorganic polyanion and crystal lattice packing considerations. Interestingly, strong octahedral distortions around Bi^{3+} cations are also observed in oxychalcogenides such as $A_2O_2Bi_2Se_3$ (A = Sr, Ba)[41] and $LaOBiS_2$,[42] in which coordination environment around bismuth is described as square pyramidal. However, as mentioned above, since the elongated Bi – I distance in iodobismuthates is only slightly longer (<7%) than the sum of Shannon ionic radii of Bi^{3+} and I^-, and therefore, the structures are typically described as made of distorted BiI_6 octahedra. Of importance is the fact that subtle distortions of metal polyhedra, bond distances and angles can have strong influence on the observed optical and electronic properties such as optical band gaps and luminescence properties.[1, 39, 43-46]

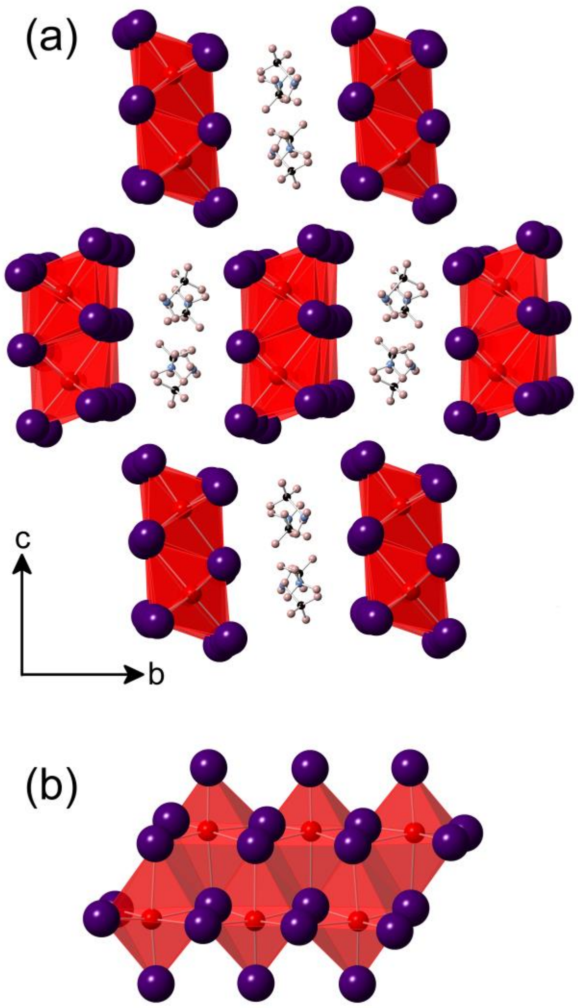

Fig. 1 (a) A polyhedral representation of the crystal structure of $(MA)_4Bi_6I_{22}$ showing $[Bi_6I_{22}]^{4-}$ clusters separated by MA^+ cations. (b) A close view of the anionic $[Bi_6I_{22}]^{4-}$ cluster formed by six octahedral BiI_6 units sharing common edges.

Stability Studies. Hybrid organic−inorganic halide compounds are known to display lower thermal stability compared all-inorganic compositions. In line with this general observation, $(MA)_4Bi_6I_{22}$ undergoes a decomposition at 145 °C, resulting in a 1.5% weight loss, which corresponds to the loss of half of CH_3NH_2 (two) per formula unit (Fig. 2). Another endothermic peak appears at 195 °C, which however is not accompanied by a weight loss and is tentatively assigned to a melting transition. The enthalpies associated with decomposition at 146 ˚C and melting at 195˚C are 1.39 J/g and 25.39 J/g, respectively. Positive enthalpy values are in agreement with two assigned endothermic transitions. A complete decomposition of the material and evaporation occurs above 300 °C. In comparison, $(MA)_3Bi_2I_9$ shows a single step decomposition above 327 °C.[47]

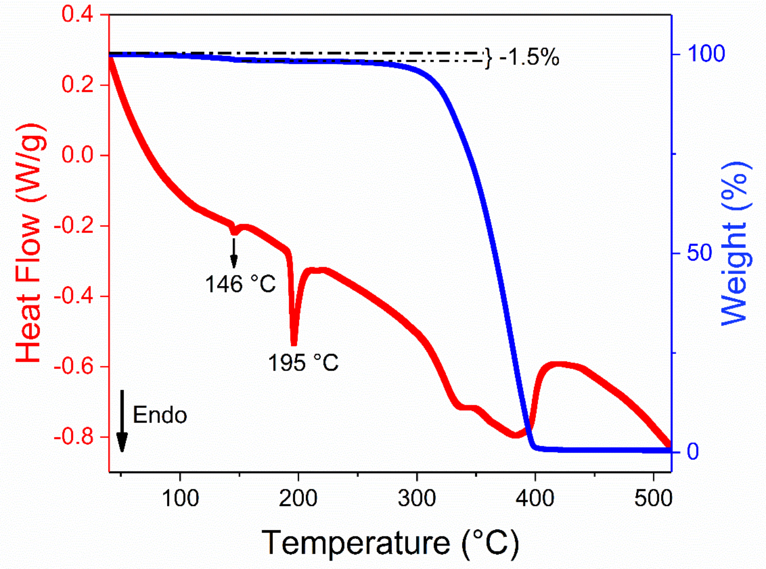

Fig. 2 Thermogravimetric Analysis (TGA) and differential scanning calorimetry (DSC) measurement results for $(MA)_4Bi_6I_{22}$.

The described synthetic procedure yields sizeable single crystals (Fig. S1) that are free of impurity inclusions (Fig. S3). However, we noticed the emergence of BiI_3 impurity peaks in the powder X-ray diffraction (PXRD) patterns upon grinding the crystals (Fig. S4). A similar sample degradation upon grinding was recently reported for methylammonium gold halides.[48] Furthermore, stability of $(MA)_4Bi_6I_{22}$ crystals with respect to ambient air and moisture was studied through periodic PXRD measurements (Fig. S5). Within 2 weeks, an unknown impurity peak emerges in the measured PXRD patterns (Fig. S5), suggesting limited ambient air stability of this material both in polycrystalline and single crystal forms.

Optical Properties $(MA)_4Bi_6I_{22}$ was studied photophysically using diffuse reflectance, photoluminescence excitation (PLE), and photoluminescence (PL) spectroscopies. Pseudoabsorption data was obtained by transforming the diffuse reflectance data using the Kubelka−Munk function (F(R)), as shown in Fig. 3a. The F(R) plot shows a band-to-band absorption feature at 1.89 eV (later confirmed with PL), which falls in the energy range of 1.77 - 1.93 eV expected for red colored crystals. The Kubelka-Munk pseudoabsoprtion data can be used to evaluate direct or indirect nature of the optical band gap through the Tauc analysis. For $(MA)_4Bi_6I_{22}$, the indirect and direct band gap fittings yield comparable 1.87 and 1.95 eV band gaps, respectively. In combination with the band structure calculations results (vide infra), we estimate an indirect band gap value of 1.9 eV for $(MA)_4Bi_6I_{22}$. This value is lower than ~ 2eV for $(MA)_3Bi_2I_9$ and is comparable to the band gaps reported for other known iodobismuthates, which are in the 1.9 – 2.5 eV range.[39, 47]

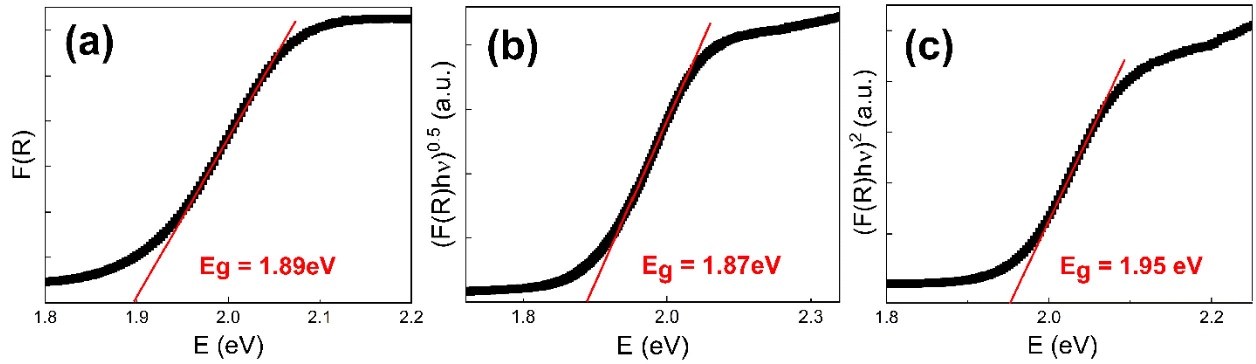

Fig. 3 (a) Optical absorption data for $(MA)_4Bi_6I_{22}$ shown using Kubelka-Munk function, F(R), plotted against photon energy. Tauc plots are drawn assuming (b) indirect direct and (c) direct band gaps.

Upon 325 nm laser excitation, photoluminescence spectra of $(MA)_4Bi_6I_{22}$ shows a red emission with a maximum at 1.92 eV at lower temperatures (Fig. 4). This emission corresponds to band-to-band charge recombination and confirms the assigned band gap of ~1.9 eV based on optical absorption measurements. However, above 120 K, rapid thermal quenching of PL results in no observable room temperature emission. Such weak emission at room temperature can be attributed to the indirect nature of the band gap in $(MA)_4Bi_6I_{22}$ (see DFT results below). In addition, we note that other recently reported iodobismuthates also have weak or negligible PL emission at room temperature.[47, 49, 50] Based on the temperature dependent PL measurements, we plotted in Fig S6, the thermal evolution of the PL peak position and the integrated PL intensity. Upon heating, the maximum emission first red shifts until between 2 and 15K (region A), then stabilizes between 15 and 40K (region B), and finally significantly red shifts above 40 K (region C) and become quite constant at temperature higher than 60K. Similarly, the integrated PL intensity shows a "three steps" temperature dependent behavior. A significant quenching is observed in region A, then a slight intensity decrease was noticed in region B. However, in region C, the integrated PL intensity become very weak and constant. This complicated temperature-dependent PL behavior was previously observed in several similar hybrid metal halides and is often explained by the presence of structural phase transition that affect the band structure of the materials and their optical properties.[51-53] However, the presence of structural phase transition for $(MA)_4Bi_6I_{22}$ is ruled out based on the heat capacity measurements (see below). Therefore, such a PL behavior change can result from irregular unit cell contractions at low temperature, which can impact the band gap of the materials .[39]

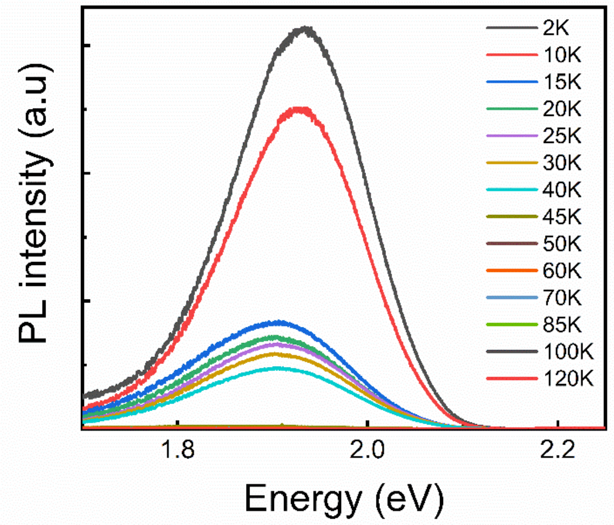

Fig. 4 Temperature-dependent PL data from 2 to 120 K.

Interestingly, $(MA)_4Bi_6I_{22}$ demonstrates color change from dark red to orange on cooling. To check if structural phase transitions might be the origin of the observed thermochromism, heat capacity of $(MA)_4Bi_6I_{22}$ was measured from 2 to 270 K. The overall shape of Cp(T) curve (see Fig. S6) is typical for non-magnetic wide-gap insulators without phase transitions (within the limitation of the experimental method used). At low temperatures, the Cp(T) variation of $(MA)_4Bi_6I_{22}$ can be well described by the formula: $Cp(T) = \gamma T + \beta T^3$, with the coefficients $\gamma \approx 0$ and $\beta = 96.3$ mJ/mol K^4. The electronic contribution to the specific heat is very close to zero, in accordance with the presence of an insulating ground state in this material (zero densities of states at the Fermi level). From the value of β one estimates the Debye temperature (T_D) to be about 85 K. The results of heat capacity measurements are supported by our powder and single crystal X-ray diffraction measurements at 100 K and room temperature. It is worth mentioning that the heat capacity value at room temperature is about 650 J/mol K, and it is lower than the expected value estimated by the Dulong-Petit law for these materials (~800 J/molK, assuming rigid MA units and Bi and I atoms). Interestingly, a similar behavior has been observed for systems containing light atoms that are strongly bonded to each other, causing some vibrational modes to be unpopulated even at 300 K due to their high vibrational frequencies.[54] This indicates the presence of complex vibrational behavior in this material with strong anharmonicity,[55] which should be studied further by other techniques such as inelastic neutron scattering. In general , beyond structural phase transitions, thermochromism can also be induced by subtle changes to the bond distances and angles in metal halides such as in the case of the related iodobismuthates featuring isolated $[Bi_3I_{11}]^{2-}$ anions.[39] Such regular changes to the bond lengths and angles upon regular unit cell contraction on cooling can impact the materials band gap , and subsequently, onset of optical absorption, which explains the observed change in color.[56]

Electronic Band Structure Calculations. The calculated electronic structure of $(MA)_4Bi_6I_{22}$ (Fig. 5) shows that the valence band is mainly made up of I-5p orbitals while the conduction band has strong components from both Bi-6p and I-5p. Both the valence and conduction bands are flat, indicating weak coupling between Bi_6I_{22} clusters in agreement with the 0D crystal structure of this material. The conduction band minimum (CBM) is at the X point while the valence band maximum (VBM) is located between the Γ and the Z. The energy of the VBM is higher than the energy of the highest occupied band at the X point by only 0.02 eV. Therefore, the band gap is slightly indirect. The calculated band gap is 1.45 eV at the PBE level, which is underestimated due to the well-known PBE band gap error.

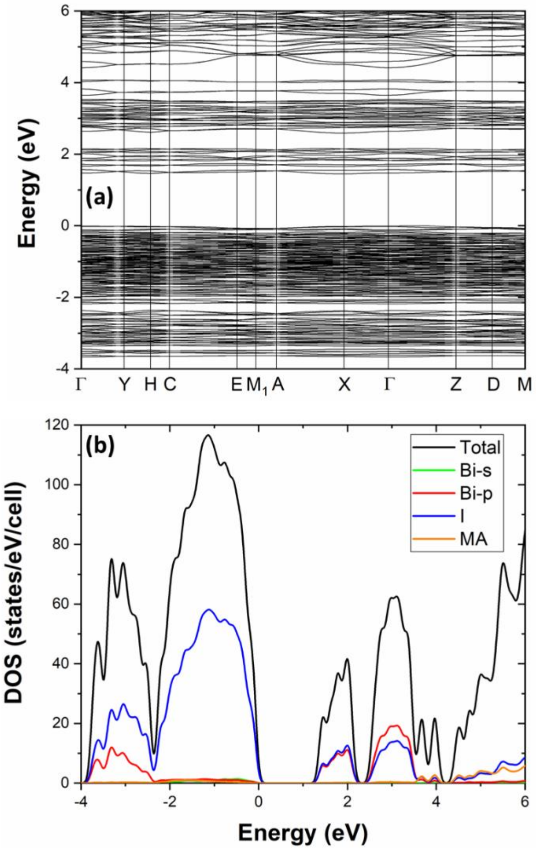

Fig. 5 (a) Electronic band structure and (2) density of states (DOS) of $(MA)_4Bi_6I_{22}$ calculated using PBE functionals.

Conclusions

In conclusion, impurity-assisted synthesis and properties of a brand-new compound in the MA-Bi-I phase diagram is reported. In the absence of the HgI_2 impurity, solution reactions yield $(MA)_3Bi_2I_9$, which is a high stability phase in this phase diagram. $(MA)_4Bi_6I_{22}$ adopts a 0D crystal structure featuring hexameric $[Bi_6I_{22}]^{4-}$ polyanionic clusters that are separated by MA^+ cations.

Optical absorption measurements and electronic structure calculations suggest a slightly indirect band gap of 1.9 eV for $(MA)_4Bi_6I_{22}$. Low temperature photoluminescence spectra contain a single peak at 636 nm attributed to band-to-band charge recombination at the bandgap. Importantly, this work suggests that through the utilization of various impurity additives in solution reactions, the chemistry of iodobismuthates can be greatly expanded to include otherwise inaccessible compounds.

Conflicts of interest

There are no conflicts to declare.

Acknowledgements

We acknowledge the financial support for this work provided by the University of Oklahoma startup funds and by a grant from Oklahoma Center for the Advancement of Science and Technology (OCAST) under grant AR18-008. M.-H.D. was supported by the U.S. Department of Energy, Office of Science, Basic Energy Sciences, Materials Sciences and Engineering Division. K.G. acknowledges support from the U.S. DOE's Early Career Research Program. X.D. acknowledges support from INL's LDRD program (19P43-013FP). We thank Dr. Douglas R.

Powell for his help with the single crystal X-ray diffraction measurements (supported by NSF grant CHE-1726630).

Footnotes

Electronic supplementary information (ESI) available: Supporting figures and tables.

Notes and references

1. B. Saparov and D. B. Mitzi, Organic–Inorganic Perovskites: Structural Versatility for Functional Materials Design, *Chemical Reviews*, 2016, **116**, 4558-4596.
2. G. A. Fisher and N. C. Norman, in *Advances in Inorganic Chemistry*, ed. A. G. Sykes, Academic Press, 1994, vol. 41, pp. 233-271.
3. M.-W. Yuan, L.-H. Li and L. Chen, Syntheses, Structures, and Theoretical Studies of New Mercury Iodobismuthates: (Et4N)4(Bi4Hg2I20) and (nBu4N)2(Bi2HgI10), *Zeitschrift für anorganische und allgemeine Chemie*, 2009, **635**, 1645-1649.
4. A. Yangui, R. Roccanova, Y. Wu, M.-H. Du and B. Saparov, Highly Efficient Broad-Band Luminescence Involving Organic and Inorganic Molecules in a Zero-Dimensional Hybrid Lead Chloride, *J. Phys. Chem. C*, 2019, **123**, 22470-22477.
5. N. Leblanc, N. Mercier, L. Zorina, S. Simonov, P. Auban-Senzier and C. Pasquier, Large Spontaneous Polarization and Clear Hysteresis Loop of a Room-Temperature Hybrid Ferroelectric Based on Mixed-Halide [BiI3Cl2] Polar Chains and Methylviologen Dication, *J. Am. Chem. Soc.*, 2011, **133**, 14924-14927.
6. D. B. Mitzi, C. A. Feild, W. T. A. Harrison and A. M. Guloy, Conducting tin halides with a layered organic-based perovskite structure, *Nature*, 1994, **369**, 467-469.
7. E. Lifshitz, M. Yassen, L. Bykov, I. Dag and R. Chaim, Nanometer-sized particles of lead iodide embedded in silica films, *The Journal of Physical Chemistry*, 1994, **98**, 1459-1463.
8. J. S. Manser, J. A. Christians and P. V. Kamat, Intriguing Optoelectronic Properties of Metal Halide Perovskites, *Chemical Reviews*, 2016, **116**, 12956-13008.
9. L. Mazzarella, Y.-H. Lin, S. Kirner, A. B. Morales-Vilches, L. Korte, S. Albrecht, E. Crossland, B. Stannowski, C. Case, H. J. Snaith and R. Schlatmann, Infrared Light Management Using a Nanocrystalline Silicon Oxide Interlayer in Monolithic Perovskite/Silicon Heterojunction Tandem Solar Cells with Efficiency above 25%, *Adv. Energy Mater.*, 2019, **9**, 1803241.
10. M. Sharma, A. Yangui, V. R. Whiteside, I. R. Sellers, D. Han, S. Chen, M.-H. Du and B. Saparov, Rb4Ag2BiBr9: A Lead-Free Visible Light Absorbing Halide Semiconductor with Improved Stability, *Inorg. Chem.*, 2019, DOI: 10.1021/acs.inorgchem.8b03623.
11. G. Hodes and D. Cahen, Perovskite cells roll forward, *Nat. Photon.*, 2014, **8**, 87.
12. M. Lyu, J.-H. Yun, P. Chen, M. Hao and L. Wang, Addressing Toxicity of Lead: Progress and Applications of Low-Toxic Metal Halide Perovskites and Their Derivatives, *Adv. Energy Mater.*, 2017, **7**, 1602512.
13. B. Saparov, J.-P. Sun, W. Meng, Z. Xiao, H.-S. Duan, O. Gunawan, D. Shin, I. G. Hill, Y. Yan and D. B. Mitzi, Thin-Film Deposition and Characterization of a Sn-Deficient Perovskite Derivative Cs2SnI6, *Chem. Mater.*, 2016, **28**, 2315-2322.
14. T. C. Jellicoe, J. M. Richter, H. F. J. Glass, M. Tabachnyk, R. Brady, S. E. Dutton, A. Rao, R. H. Friend, D. Credgington, N. C. Greenham and M. L. Böhm, Synthesis and Optical Properties of Lead-Free Cesium Tin Halide Perovskite Nanocrystals, *J. Am. Chem. Soc.*, 2016, **138**, 2941-2944.
15. B. Saparov, F. Hong, J.-P. Sun, H.-S. Duan, W. Meng, S. Cameron, I. G. Hill, Y. Yan and D. B. Mitzi, Thin-Film Preparation and Characterization of Cs3Sb2I9: A Lead-Free Layered Perovskite Semiconductor, *Chem. Mater.*, 2015, **27**, 5622-5632.

16. F. Jiang, D. Yang, Y. Jiang, T. Liu, X. Zhao, Y. Ming, B. Luo, F. Qin, J. Fan, H. Han, L. Zhang and Y. Zhou, Chlorine-Incorporation-Induced Formation of the Layered Phase for Antimony-Based Lead-Free Perovskite Solar Cells, *J. Am. Chem. Soc.*, 2018, **140**, 1019-1027.
17. Q. Sun, H. Chen and W.-J. Yin, Do Chalcogenide Double Perovskites Work as Solar Cell Absorbers: A First-Principles Study, *Chem. Mater.*, 2019, **31**, 244-250.
18. N. Mercier, N. Louvain and W. Bi, Structural diversity and retro-crystal engineering analysis of iodometalate hybrids, *CrystEngComm*, 2009, **11**, 720-734.
19. R. Roccanova, W. Ming, V. R. Whiteside, M. A. McGuire, I. R. Sellers, M.-H. Du and B. Saparov, Synthesis, Crystal and Electronic Structures, and Optical Properties of (CH3NH3)2CdX4 (X = Cl, Br, I), *Inorg. Chem.*, 2017, **56**, 13878-13888.
20. F. Wei, Z. Deng, S. Sun, F. Zhang, D. M. Evans, G. Kieslich, S. Tominaka, M. A. Carpenter, J. Zhang, P. D. Bristowe and A. K. Cheetham, Synthesis and Properties of a Lead-Free Hybrid Double Perovskite: (CH3NH3)2AgBiBr6, *Chem. Mater.*, 2017, **29**, 1089-1094.
21. Z. Xiao, W. Meng, J. Wang, D. B. Mitzi and Y. Yan, Searching for promising new perovskite-based photovoltaic absorbers: the importance of electronic dimensionality, *Materials Horizons*, 2017, **4**, 206-216.
22. L.-M. Wu, X.-T. Wu and L. Chen, Structural overview and structure–property relationships of iodoplumbate and iodobismuthate, *Coordination Chemistry Reviews*, 2009, **253**, 2787-2804.
23. H. Li, C. Wu, Y. Yan, B. Chi, J. Pu, J. Li and S. Priya, Fabrication of Lead-Free (CH3NH3)3Bi2I9 Perovskite Photovoltaics in Ethanol Solvent, *ChemSusChem*, 2017, **10**, 3994-3998.
24. Z. Zhang, X. Li, X. Xia, Z. Wang, Z. Huang, B. Lei and Y. Gao, High-Quality (CH3NH3)3Bi2I9 Film-Based Solar Cells: Pushing Efficiency up to 1.64%, *J. Phys. Chem. Lett.*, 2017, **8**, 4300-4307.
25. B.-W. Park, B. Philippe, X. Zhang, H. Rensmo, G. Boschloo and E. M. J. Johansson, Bismuth Based Hybrid Perovskites A3Bi2I9 (A: Methylammonium or Cesium) for Solar Cell Application, *Adv. Mater.*, 2015, **27**, 6806-6813.
26. F. Hong, B. Saparov, W. Meng, Z. Xiao, D. B. Mitzi and Y. Yan, Viability of Lead-Free Perovskites with Mixed Chalcogen and Halogen Anions for Photovoltaic Applications, *J. Phys. Chem. C*, 2016, **120**, 6435-6441.
27. T. T. Tran, M. A. Quintero, K. E. Arpino, Z. A. Kelly, J. R. Panella, X. Wang and T. M. McQueen, Chemically controlled crystal growth of (CH3NH3)2AgInBr6, *CrystEngComm*, 2018, **20**, 5929-5934.
28. N. J. Jeon, J. H. Noh, Y. C. Kim, W. S. Yang, S. Ryu and S. I. Seok, Solvent engineering for high-performance inorganic–organic hybrid perovskite solar cells, *Nature Materials*, 2014, **13**, 897.
29. G. Kresse and J. Furthmüller, Efficiency of ab-initio total energy calculations for metals and semiconductors using a plane-wave basis set, *Computational Materials Science*, 1996, **6**, 15-50.
30. G. Kresse and D. Joubert, From ultrasoft pseudopotentials to the projector augmented-wave method, *Physical Review B*, 1999, **59**, 1758.
31. J. P. Perdew, K. Burke and M. Ernzerhof, Generalized gradient approximation made simple, *Physical review letters*, 1996, **77**, 3865.

32. Y. Peng, L. Li, C. Ji, Z. Wu, S. Wang, X. Liu, Y. Yao and J. Luo, Tailored Synthesis of an Unprecedented Pb–Mn Heterometallic Halide Hybrid with Enhanced Emission, *J. Am. Chem. Soc.*, 2019, **141**, 12197-12201.
33. R. L. Z. Hoye, R. E. Brandt, A. Osherov, V. Stevanović, S. D. Stranks, M. W. B. Wilson, H. Kim, A. J. Akey, J. D. Perkins, R. C. Kurchin, J. R. Poindexter, E. N. Wang, M. G. Bawendi, V. Bulović and T. Buonassisi, Methylammonium Bismuth Iodide as a Lead-Free, Stable Hybrid Organic–Inorganic Solar Absorber, *Chemistry – A European Journal*, 2016, **22**, 2605-2610.
34. M. Pazoki, M. B. Johansson, H. Zhu, P. Broqvist, T. Edvinsson, G. Boschloo and E. M. J. Johansson, Bismuth Iodide Perovskite Materials for Solar Cell Applications: Electronic Structure, Optical Transitions, and Directional Charge Transport, *J. Phys. Chem. C*, 2016, **120**, 29039-29046.
35. P. S. Whitfield, N. Herron, W. E. Guise, K. Page, Y. Q. Cheng, I. Milas and M. K. Crawford, Structures, Phase Transitions and Tricritical Behavior of the Hybrid Perovskite Methyl Ammonium Lead Iodide, *Sci. Rep*, 2016, **6**, 35685.
36. A. M. Goforth, L. Peterson, M. D. Smith and H.-C. zur Loye, Syntheses and crystal structures of several novel alkylammonium iodobismuthate materials containing the 1,3-bis-(4-piperidinium)propane cation, *Journal of Solid State Chemistry*, 2005, **178**, 3529-3540.
37. S. Pohl, M. Peters, D. Haase and W. Saak, *Journal*, 1994, **49**, 741.
38. W. Clegg, R. John Errington, G. A. Fisher, M. E. Green, D. C. R. Hockless and N. C. Norman, A Phosphine Complex of Bismuth(III): X-ray Crystal Structure of [PMe3H][Bi2Br7(PMe3)2], *Chemische Berichte*, 1991, **124**, 2457-2459.
39. A. M. Goforth, M. A. Tershansy, M. D. Smith, L. Peterson, J. G. Kelley, W. J. I. DeBenedetti and H.-C. zur Loye, Structural Diversity and Thermochromic Properties of Iodobismuthate Materials Containing d-Metal Coordination Cations: Observation of a High Symmetry [Bi3I11]2− Anion and of Isolated I− Anions, *J. Am. Chem. Soc.*, 2011, **133**, 603-612.
40. R. Shannon, Revised effective ionic radii and systematic studies of interatomic distances in halides and chalcogenides, *Acta Crystallographica Section A*, 1976, **32**, 751-767.
41. J. R. Panella, J. Chamorro and T. M. McQueen, Synthesis and Structure of Three New Oxychalcogenides: A2O2Bi2Se3 (A = Sr, Ba) and Sr2O2Sb2Se3, *Chem. Mater.*, 2016, **28**, 890-895.
42. R. Sagayama, H. Sagayama, R. Kumai, Y. Murakami, T. Asano, J. Kajitani, R. Higashinaka, T. D. Matsuda and Y. Aoki, Symmetry Lowering in LaOBiS2: A Mother Material for BiS2-Based Layered Superconductors, *Journal of the Physical Society of Japan*, 2015, **84**, 123703.
43. R. Roccanova, A. Yangui, G. Seo, T. D. Creason, Y. Wu, D. Y. Kim, M.-H. Du and B. Saparov, Bright Luminescence from Nontoxic CsCu2X3 (X = Cl, Br, I), *ACS Materials Letters*, 2019, **1**, 459-465.
44. A. Yangui, R. Roccanova, T. M. McWhorter, Y. Wu, M.-H. Du and B. Saparov, Hybrid Organic–Inorganic Halides (C5H7N2)2MBr4 (M = Hg, Zn) with High Color Rendering Index and High-Efficiency White-Light Emission, *Chem. Mater.*, 2019, **31**, 2983-2991.
45. R. Roccanova, A. Yangui, H. Nhalil, H. Shi, M.-H. Du and B. Saparov, Near-Unity Photoluminescence Quantum Yield in Blue-Emitting Cs3Cu2Br5–xIx ($0 \le x \le 5$), *ACS Applied Electronic Materials*, 2019, **1**, 269-274.

46. R. Roccanova, M. Houck, A. Yangui, D. Han, H. Shi, Y. Wu, D. T. Glatzhofer, D. R. Powell, S. Chen, H. Fourati, A. Lusson, K. Boukheddaden, M.-H. Du and B. Saparov, Broadband Emission in Hybrid Organic–Inorganic Halides of Group 12 Metals, *ACS Omega*, 2018, **3**, 18791-18802.
47. J. Zhang, S. Han, C. Ji, W. Zhang, Y. Wang, K. Tao, Z. Sun and J. Luo, [(CH3)3NH]3Bi2I9: A Polar Lead-Free Hybrid Perovskite-Like Material as a Potential Semiconducting Absorber, *Chemistry – A European Journal*, 2017, **23**, 17304-17310.
48. C. Worley, A. Yangui, R. Roccanova, M.-H. Du and B. Saparov, (CH3NH3)AuX4·H2O (X=Cl, Br) and (CH3NH3)AuCl4: Low-Band Gap Lead-Free Layered Gold Halide Perovskite Materials, *Chemistry – A European Journal*, 2019, **25**, 9875-9884.
49. I. W. H. Oswald, E. M. Mozur, I. P. Moseley, H. Ahn and J. R. Neilson, Hybrid Charge-Transfer Semiconductors: (C7H7)SbI4, (C7H7)BiI4, and Their Halide Congeners, *Inorg. Chem.*, 2019, **58**, 5818-5826.
50. N. A. Yelovik, A. V. Mironov, M. A. Bykov, A. N. Kuznetsov, A. V. Grigorieva, Z. Wei, E. V. Dikarev and A. V. Shevelkov, Iodobismuthates Containing One-Dimensional BiI4– Anions as Prospective Light-Harvesting Materials: Synthesis, Crystal and Electronic Structure, and Optical Properties, *Inorg. Chem.*, 2016, **55**, 4132-4140.
51. A. Yangui, S. Pillet, E.-E. Bendeif, A. Lusson, S. Triki, Y. Abid and K. Boukheddaden, Broadband Emission in a New Two-Dimensional Cd-Based Hybrid Perovskite, *ACS Photonics*, 2018, **5**, 1599-1611.
52. A. Yangui, S. Pillet, A. Mlayah, A. Lusson, G. Bouchez, S. Triki, Y. Abid and K. Boukheddaden, Structural phase transition causing anomalous photoluminescence behavior in perovskite (C6H11NH3)2[PbI4], *The Journal of Chemical Physics*, 2015, **143**, 224201.
53. A. Yangui, S. Pillet, D. Garrot, S. Triki, Y. Abid and K. Boukheddaden, Evidence and detailed study of a second-order phase transition in the (C6H11NH3)2[PbI4] organic-inorganic hybrid material, *Journal of Applied Physics*, 2015, **117**, 115503.
54. M. Laing and M. Laing, Dulong and Petit's Law: We Should Not Ignore Its Importance, *Journal of Chemical Education*, 2006, **83**, 1499.
55. E. A. Stern, Theory of the Anharmonic Properties of Solids, *Phys. Rev.*, 1958, **111**, 786-797.
56. B. Sun, X.-F. Liu, X.-Y. Li, Y. Cao, Z. Yan, L. Fu, N. Tang, Q. Wang, X. Shao, D. Yang and H.-L. Zhang, Reversible Thermochromism and Strong Ferromagnetism in Two-Dimensional Hybrid Perovskites, *Angew. Chem. Int. Ed.*, **59**, 203-208.

TOC entry

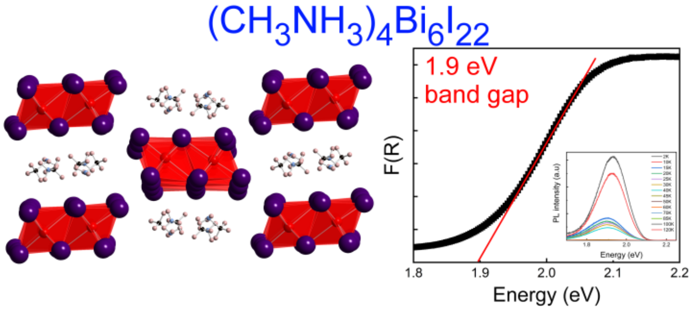

A novel iodobismuthate semiconductor $(MA)_4Bi_6I_{22}$ (measured bandgap of 1.9 eV) was prepared using solution methods in the presence of HgI_2 additive.